Environmental Earth Sciences (2022) 81:243
https://doi.org/10.1007/s12665-022-10364-2

ORIGINAL ARTICLE

Experimental research on deformation failure process of roadway tunnel in fractured rock mass induced by mining excavation

Guang Li[1,2,3] · Fengshan Ma[1,2] · Jie Guo[1,2] · Haijun Zhao[1,2]

Received: 16 November 2020 / Accepted: 19 March 2022 / Published online: 13 April 2022

Abstract

Deformation failure of roadways in fractured rock can lead to large-volume collapse and other engineering accidents. Failure mechanisms in fractured rock are complex and poorly understood, so to explore this issue, we simulated fractured rock masses using physical model tests in combination with numerical computations. A set of experimental techniques for roadway excavation under jointed surrounding rock included a mixed pouring–bricking method and a roadway excavation device, which can reproduce the structural characteristics of the prototype and replicate the excavation conditions of the roadway. Stress distribution characteristics of the roadway, from loading to excavation, were obtained based on strain monitoring and image acquisition, and the process of roadway deformation and failure was described in detail. A series of numerical simulations were conducted to investigate the deformation failure mechanisms of roadways under different excavation conditions. Results indicate that the deformation failure modes of roadways including collapse, rock burst, and floor heaving that were similar regardless of depth. Deformation failure modes of the roadway were determined by rock mass structure, and the deformation intensity was determined by geo-stress. Model testing and numerical simulation were consistent; hence, findings provide a theoretical basis and technical guidance for roadway engineering in fractured rock masses.

Keywords Roadway deformation failure · Jointed rock mass · Physical model test · PFC^{2D}

Introduction

Roadways are the lifeline of successful mining projects because they are critical for personnel operation, infrastructure construction, and ore transportation. With greater mining depth, roadways may deteriorate and result in a series of engineering disasters, such as large deformation of rock mass, long-time rheology of roadway, roof collapse, floor uplift, and rock burst, which become increasingly serious (Ren et al. 2020). It is especially difficult to apply the deformation failure law for fractured rock bodies, and to engineer efficient support modes for safe and cost effective projects.

✉ Fengshan Ma
fsma@mail.iggcas.ac.cn

[1] Key Laboratory of Shale Gas and Geoengineering, Institute of Geology and Geophysics, Chinese Academy of Sciences, Beijing 100029, China

[2] Innovation Academy for Earth Science, CAS, Beijing 100029, China

[3] University of Chinese Academy of Sciences, Beijing 100049, China

Roadway deformation and stability research mainly rely on field investigation, theoretical analysis, numerical simulation, and physical model tests. However, it is expensive and laborious to conduct a detailed field investigation because there are numerous factors affecting deformation in a complex fractured rock body (Xu et al. 2019). An extreme simplification and a number of assumptions are unavoidable for the prototype before the theoretical analysis, and it is very difficult to describe engineering-scale problems with mathematical models (Tu et al. 2018). In contrast, physical experiments can replicate the whole process from elasticity deformation to destruction under complex conditions. However, numerical techniques that are characterized by economy and high efficiency have made great progress, and the simulation results can be mutually verified with the experimental results (Shreedharan et al. 2016).

In recent years, a large number of physical model tests have been conducted to examine the deformation failure laws of roadway under different excavation conditions. Hendron et al. (1972) studied the mechanical behavior of jointed rock roadway under static load. Norman (1981) used a small brittle model to study the deformation failure mechanism of

coal mine roadway. Lee and Schubert (2008) conducted experimental research on the deformation failure mechanism of soft rock roadway surface. Gou et al. (2009) built two physical models based on the self-developed model test system and discussed roadway deformation failure under different horizontal stresses. These studies showed that the roof and floor of the roadway are the key supporting parts. He et al. (2009) combined infrared thermal imaging system with physical model test to study the impact of strata dip angle and temperature in the excavation process of mining roadway. Zhang et al. (2010) evaluated deformation characteristics, fracture evolution process, and displacement distribution of an inclined and layered surrounding rock roadway under different stress conditions, and proposed an optimal support method. Huang et al. (2013) investigated the role of soft structural planes in the roadway deformation failure process, and put forward several different failure modes. Li et al. (2015) studied the special working condition of a deep thick coal roadway and revealed the distribution characteristics of surrounding rock displacement and stress in the whole excavation process.

Fakhimi et al. (2002) and Wang et al. (2003) used Particle Flow Code (PFC) to simulate deformation failure of circular roadways after excavation. Cai et al. (2007) obtained acoustic emission characteristics of surrounding rock during excavation in large underground engineering projects. An and Tannant (2007) discussed the deformation failure characteristics of roadway under dynamic loading. Wang and Tian (2018) analyzed the failure mechanical mechanism and crack evolution process of surrounding rock mass in coal strata under different conditions. Liu et al. (2019) established a horseshoe-shaped roadway model, compared the distribution of force chain, displacement and strain in the model results, and proposed four zones in the roadway deformation process.

However, in the previous studies, most of the research objects were homogeneous structures or layered structures, and there are few studies on the excavation of roadways having multiple groups of cross joints in the surrounding rock. In this case study of the fractured roadway tunnels in Jinchuan nickel mine, China, we perform a physical model test and a numerical simulation calculation with the objectives being to obtain displacement and strain distribution laws, simulate the deformation failure process of fractured roadways, and analyze deformation failure mechanisms of roadways under different excavation conditions.

Physical model test

A physical model test is an important method for studying complex engineering geological problems, because the physical model can be used to simulate deformation from elasticity to plasticity and replicate the whole destruction process in a laboratory experiment.

Simulation prototype

Jinchuan is the largest nickel producing mine in China, with thick and deeply buried ore bodies as shown in Fig. 1. The mining area is located in Hexi Corridor, where tectonic movement is intense, ground stress is high, the rock mass is fractured, and joints and fissures are abundant. The average altitude of surface in the mining area is about + 1750 m. At present, the underground infrastructure has reached + 700 m and is buried more than 1000 m. A downward filling mining method is adopted in the Jinchuan Mine. Because of complex engineering geological conditions, roadway repair increased from 3200 m in 1999 to 18,423 m in 2019, which affected the economic benefits of the mine and safety of underground workers (Hui et al. 2019; Lu et al. 2018, 2020).

The dimensions of the horseshoe-shaped roadway were 4.5 × 4.5 m, as shown in Fig. 2. The engineering geological data in the study mine showed that the typical surrounding rock mass was rhombic marble with two sets of intersecting joints. The strike of the two sets of structural planes was nearly perpendicular, the inclination ranged from 30° to 60°, and the rock stratum thickness was about 0.5–1.5 m. The deformation failure in the surrounding rock mass was mainly controlled by the structural plane, and was unstable. Thus, the roadway under this type of surrounding rock mass was selected as the prototype in this test.

Similarity relation

Physical experiments require a similarity between the model and the prototype. However, because of high demands on materials, equipment, and technology, it is difficult to achieve complete similarity. Therefore, in general, several important indicators are selected according to the purpose

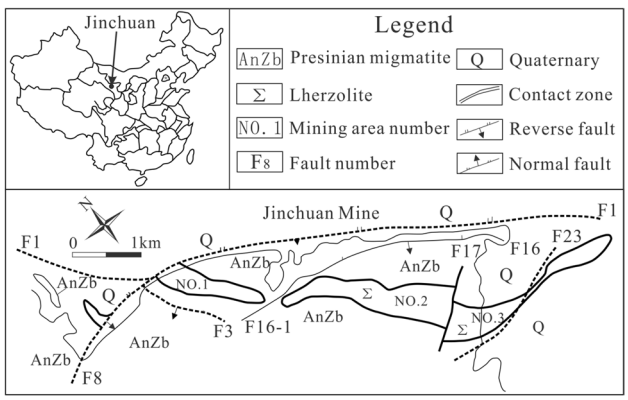

Fig. 1 Engineering geological background of the Jinchuan Mine

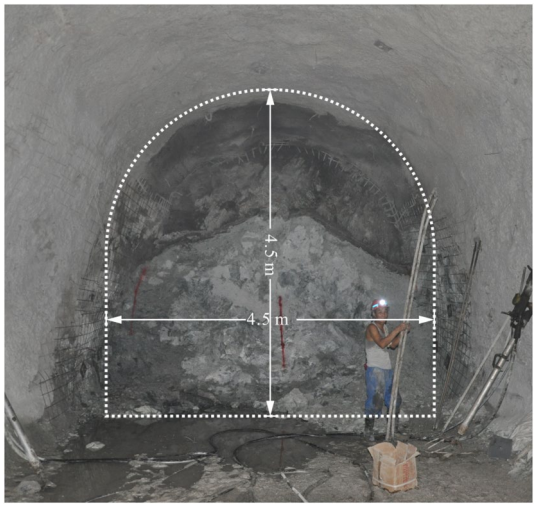

Fig. 2 Typical roadway section in Jinchuan mining area

Table 1 Physical and mechanics parameters of the rock and rock mass

Physical quantity	Similarity relation	Similarity constant
Geometry (key constant)	C_l	30
Density (key constant)	C_ρ	1.6
Displacement (key constant)	C_D	30
Poisson's ratio	$C_\mu = 1$	1
Elasticity modulus	$C_E = C_\rho C_l$	48
Strain	$C_\varepsilon = C_\rho C_l / C_E$	1
Stress	$C_\sigma = C_l C_\gamma$	48
Internal friction angle	$C_\varphi = {}_1$	1
Cohesion	$C_c = C_\rho C_l$	48
Time	$C_t = C_l (C_\rho / C_E)^{1/2}$	5.48

of the study. The ratio of the same dimensional quantities in the prototype and model was used as a similarity constant, which is indicated by the letter C.

Considering the influence of excavation stress, boundary conditions, and laboratory infrastructures, the dimensions of the physical model were 105 × 105 × 20 cm and the roadway diameter was 15 cm. Thus, the geometry similarity constant C_l is 30, and other basic physical quantities were calculated in accordance with the law of Buckingham π theorem, as shown in Table 1 (Sun et al. 2017).

A crucial part of a large-scale physical model test is quickly and accurately determining the ratio of similar materials. Most of the roadways in the study area are distributed in the marble rock mass on both sides of the ore body, and the physical and mechanical parameters of the intact marble rock and marble rock mass are shown in Table 2. River sand, cement, and gypsum were adopted as the raw materials to reduce the test cost, simplify the test procedures, and fully utilize the properties of raw materials. Then, a series of comparative tests with bone glue ratio and water–paste ratio as variables were conducted (Fig. 3). Experimental results indicate that the ratio A6 (river sand:cement = 4:1) and ratio C6 (river sand:cement:gypsum = 8:1:1) match intact marble and marble rock mass, as shown in Tables 2, 3 (Li et al. 2020a, b, c).

Model building

A physical model test is important for studying roadway stability; however, it is difficult to build similar models for jointed rock masses. Therefore, a set of physical model test methods was designed for roadway excavation under jointed surrounding rock.

For roadways excavated in the jointed surrounding rock mass, a mixed pouring–bricking method was designed. Pouring was adopted in the inner ring of the model, and bricking was used in the outer ring, which reflects the structural characteristics of jointed surrounding rocks and improves test efficiency (Fig. 4).

The joint spacing of rhombic rock masses is 0.5–1.5 m and the dip angle is 30°–60° in the study area; thus, the block was designed as 4 × 4 × 20 cm based on the

Table 2 Physical and mechanics parameters of rock mass and similar material

Lithology	Type	Density (g·cm^{-3})	Tensile strength (MPa)	Compressive strength (MPa)	Cohesion (MPa)	Internal friction angle (°)	Elastic moduli (GPa)	Poisson's ratio
Intact marble rock	Measured value	2.80–3.00	6.90–12.20	96.00–152.00	13.5–22.5	35–45	64–124	0.22–0.32
	Design value	1.75–1.88	0.14–0.25	2.00–3.29	0.28–0.47	35–45	0.88–2.58	0.22–0.32
	Ratio A6	1.82	0.43	2.62	0.24	27	0.42	0.26
Marble rock mass	Measured value	2.60–2.80	0.80–1.40	18.60–32.40	0.70–6.50	25–35	6–12	0.18–0.26
	Design value	1.63–1.75	0.02–0.03	0.39–0.68	0.04–0.14	25–35	0.13–0.25	0.18–0.26
	Ratio C6	1.75	0.18	1.42	0.14	25	0.26	0.23

Fig. 3 Parts of the samples (Li et al. 2020a, b, c)

Table 3 Mechanics parameters of the structural plane

Type	Cohesion (MPa)	Friction angle (°)
Structural plane	0.04–0.10	27–29

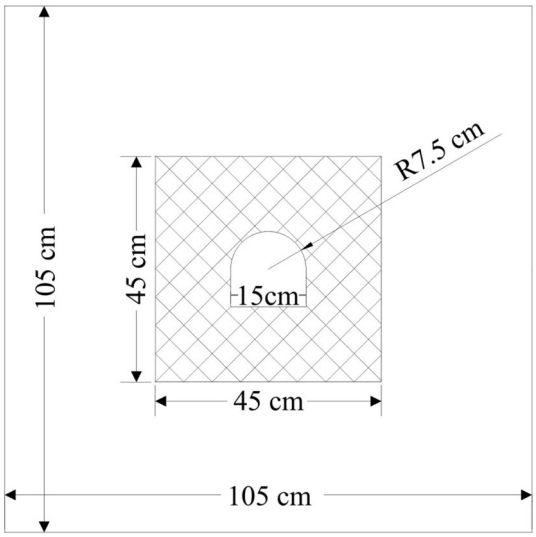

Fig. 4 Model section diagram

simulation theory. A polypropylene plastic mold, that is light and easy to demold, was made to save cost and realize mass production. After several steps including stirring, stuffing, scraping, stripping, and curing, the production of block is completed, and part of the building blocks is shown in Fig. 5.

Figure 6 shows the model building process. The outer surrounding of the model is made of similar material according to the parameters of the marble rock mass, which is compact and uniform. The material can effectively transfer stress and is conducive to observing the fracture development on the surrounding rock mass. The internal block of the model is made of similar material according to the intact marble rock, and the joints in the surrounding rock mass are clearly

Fig. 5 Building blocks

Fig. 6 Model building process

visible, which can reproduce the structural characteristics of the prototype.

In mining engineering, roadways roadway have to be excavated under the action of high in-situ stress. However, it is not easy to simulate the excavation under loading in the laboratory test. Thus, a roadway excavation device was independently developed based on embedded mold and spiral

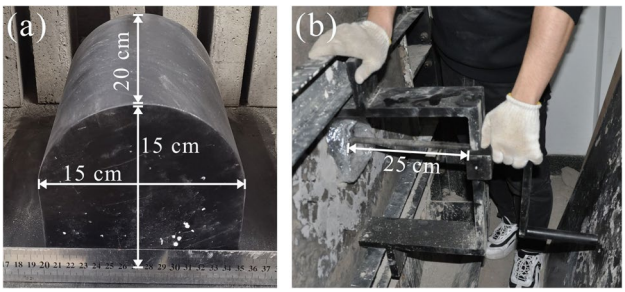

Fig. 7 Roadway excavation device; **a** embedded mold and **b** mold removal device

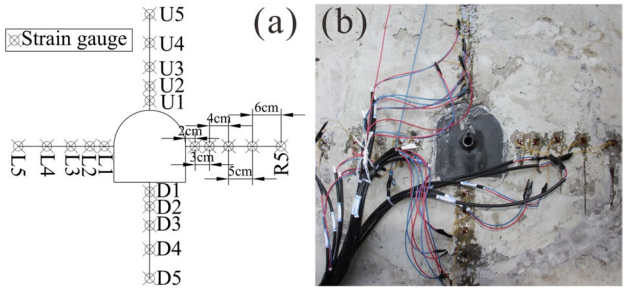

Fig. 8 Data collection devices; **a** design of the strain gauges and **b** image of the data collection devices

traction to form a roadway that would only slightly disturb the model. The embedded mold is made according to the design size of the excavated roadway, and the material is cast iron with sufficient stiffness, as shown in Fig. 7a. A nut was embedded in the middle of the mold to match the mold removal device. Through spiral traction, the embedded mold can be pulled out slowly, which is in accordance with the practice of a step-by-step excavation that only slightly disturbs the model, as shown in Fig. 7b.

Data collection

The experiment was recorded by two digital cameras, one of which took photos at regular intervals, and another one recorded the whole process. Strain gauges were installed on the back of the model to allow for observation of deformation failure on the model front. Four measuring lines including 20 gauges were set on the roof, floor, and two sides, as shown in Fig. 8.

Loading mode

The model was loaded by a self-developed hydraulic servo comprehensive experimental platform that consisted of three parts: model box, loading system, and control system, as shown in Fig. 9. The loading system was controlled using a

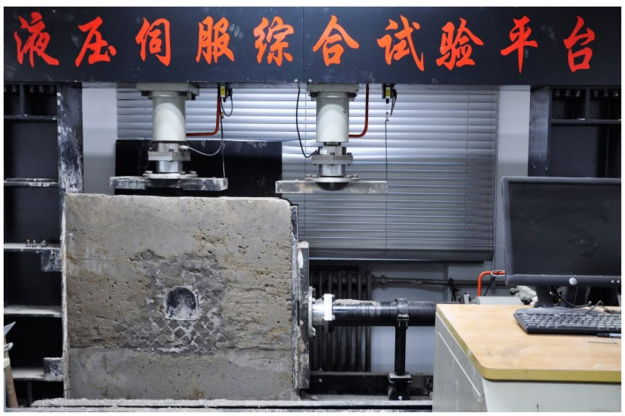

Fig. 9 Self-developed hydraulic servo comprehensive experimental platform

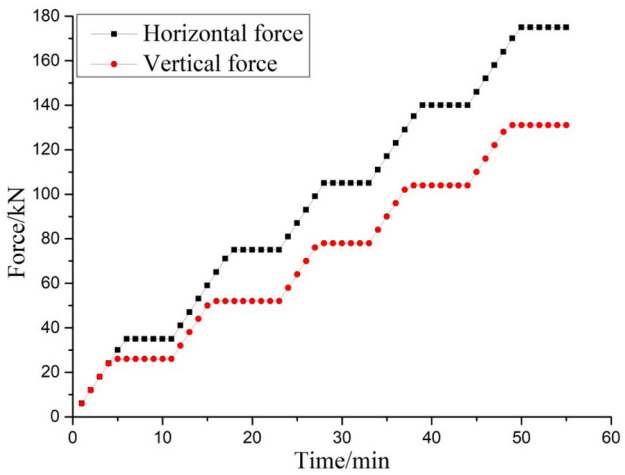

Fig. 10 Loading curves

computer, with a maximum of 300 kN loading force in the horizontal and vertical directions.

According to the actual ground stress conditions in the study area, the horizontal and vertical ground stresses were set as 40 MPa and 30 MPa, respectively. Based on the similarity relation, the horizontal force was 175 kN, and the vertical force was 131 kN. Multi-stage loading was adopted, and the interval between the two adjacent loadings was five minutes. After the loading process finished, the force was maintained for about 10 min. When the stresses on each measuring point inside the model tended to be stable and balanced, the roadway was excavated. The loading speed was 0.1 kN/s, as shown in Fig. 10.

Physical simulation results analysis

Real-time monitoring was conducted during model loading and excavation based on the strain gauges. Four strain

measuring lines were arranged on the roof, floor, and two sides of the roadway, with a total of 20 measuring points. The measuring point, R5, on the right side was destroyed during the experiment, so only 19 points were recorded, as shown in Fig. 11.

When the model is loaded, the strain data of the sensors are collected, as shown in Fig. 11. Strain data were collected for about 120 times in the test, and 'Data Collection Times' is the number of times of data collection. The strain gauge was sensitive and fragile and was easily disturbed in the test. Therefore, the shape of each curve, shown in Fig. 11, was irregular. All the points on the model showed compressive strain initially, which was the result of the preloading and the model pressure stress. At about the 69th sampling, the surrounding rock of the roadway had deformation space because of the excavation, and the compressive strain changed into tensile strain, which was also the main cause of roadway deformation and failure.

The four strain curves indicate that the strain value and deformation trend on the roof and floor were consistent. The maximum compressive strain was about 400, and the maximum tensile strain was about 1200. The pressure strain response time of the measuring points on the roof was earlier, which was induced by top loading. The strain distribution differed for the left and right sides. Responses of the measuring points on the left side were not substantial in the pressure strain stage, with compressive strain value of measuring point L1 being the only one to exceed 200; however, the value in the tensile strain stage was greater than 1200. Measuring points on the right side showed compressive strain, but tensile strain of about 500 was relatively low. The asymmetry of strain was related to the boundary effect of the model.

During the pressure strain stage, the outermost measurement point 5 generally responded first, which was determined by the stress propagation path in the model. The tensile strain was higher for measuring points closer to the goaf, which was consistent with the distribution characteristics of the loose zone in the actual engineering (Li et al. 2020a, b, c). Because the roadway was excavated from front to back and the strain gauges were glued on the back face of the model, the front part of the curve fluctuated as a result of excavation disturbance.

The entire process was recorded in the test including roadway excavation, deformation, and failure. Semi-circular arch sections were the first to deform on the two straight wall feet and the floor, because they were more prone to stress concentration, as shown in Fig. 12a. Figure 12b indicates

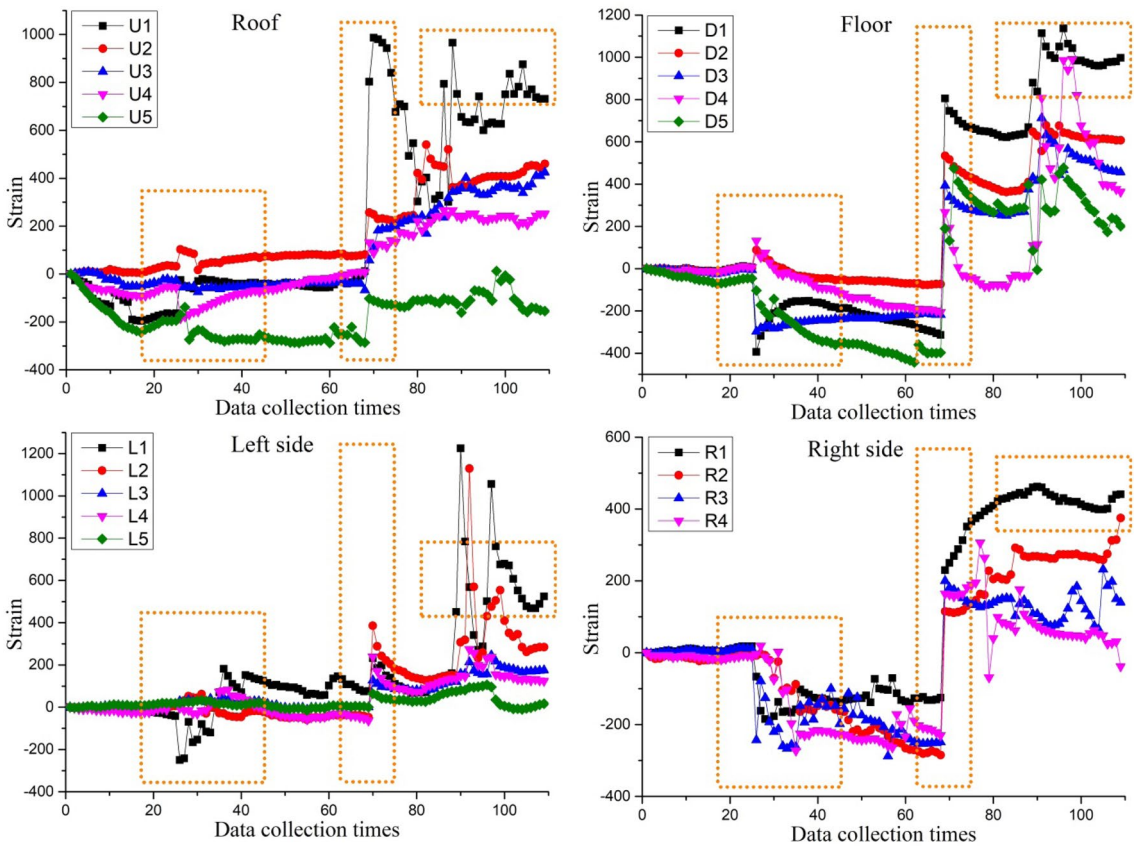

Fig. 11 Strain gauge monitoring data. Data Collection Time: the number of times of data collection

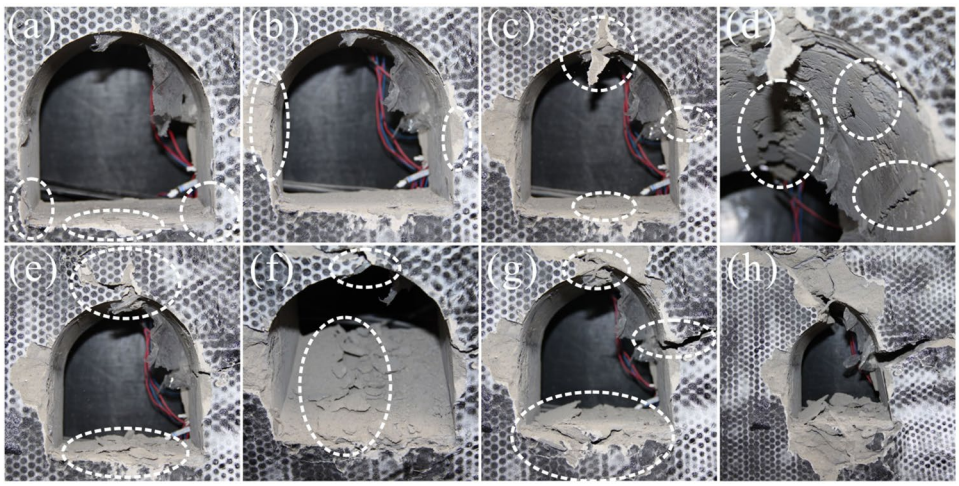

Fig. 12 Process of the roadway deformation failure; **a** deformation on the wall foot and floor; **b** failure appeared at the two sides and roof; **c** falling blocks from the roof and cracks on the sides; **d** tensile cracks on the arch shoulders and springing line; **e** serious collapse; **f** floor heaving; **g** development of the deformation failure; and **h** final state of the roadway

that local failure appeared at the two sides and roof. With continuous increase of the deformation, rock blocks fell from the roof, and tensile cracks along the roadway trend were developed on the arch shoulders and springing line, as shown in Fig. 12c and d. Next, the deformation on the roof extended to the deeper zone and the falling blocks were more serious. Collapse of this scale would seriously threaten the safety of construction workers in an actual project. Figure 12e and f showed apparent floor heaving, with serious cracking and swelling of the roadway, which was similar to the phenomenon in the field investigation. At later times, a dislocation occurred under the action of horizontal stress, so that a pointed or peach section was formed and the roadway roof was divided into two parts along a longitudinal crack. Floor heaving gradually affected the deeper rock mass, and an independent wedge uplift was developed on the floor. Fractures on the two sides constantly expanded, and deep surrounding rocks turned over and squeezed inward to the free face, as shown in Fig. 12g. Figure 12h presented the final state of the roadway at the end of the test. The surrounding rock collapse on the roof was serious and peach roof was formed because of rock mass displacement; the floor heaving was obvious, the amount of uplift was large, and the affected zone was wide; several considerable scale tensile cracks were developed on the two sides, which became the breakthroughs of the surrounding rock converged into the excavated area.

Roadways in the research area experienced severe deformation failure under the condition of no support, and the roadways could not be put into normal service with reasonable support methods. In early stage of the excavation, a timely primary support, such as bolt net and spraying, was able to limit the stress concentration deformation and collapse. Then, after a proper pressure relief, a secondary support including bolts, grouting, and rigid support could be adopted to limit the radial displacement and fully mobilize the self-bearing capacity of the surrounding rock mass. Finally, rigid supports were used to restrain creep of surrounding rock mass and ensure long-term stability of the roadway.

Numerical simulation

Discrete element method (DEM) numerical simulations were performed to further study the deformation failure mechanisms of roadways in fractured rock mass and to verify the results of the physical model test. DEM was suitable for the simulation of rock mass which was anisotropic and nonlinear (Bai and Tu 2020) using PFC^{2D} software (Itasca 2008). PFC^{2D} was selected for this because it represents the rock masses with the following characteristics:

1. Particle combinations interact with each other through boundary contact intrusion.
2. Interaction between the elements can reflect the discontinuity of a rock mass and the characteristics of common occurrence of joints.
3. Iterative calculations are adopted and large displacement and rotation are allowed.

Numerical simulation model

The numerical simulation model with size of 30×30 m was constructed based on the roadway size in Jinchuan mine, as shown in Fig. 13. The excavated roadway was a semicircular arch with a height of 4.5 m and a width of 4.5 m. There were 39,402 particles with a diameter of 6–10 cm and 70 structural planes whose inclination angle was 45° and spacing was 1.2 m. A parallel bond model (PBM) was selected, which was suitable for the mechanical analysis of rock materials (Liu et al. 2020).

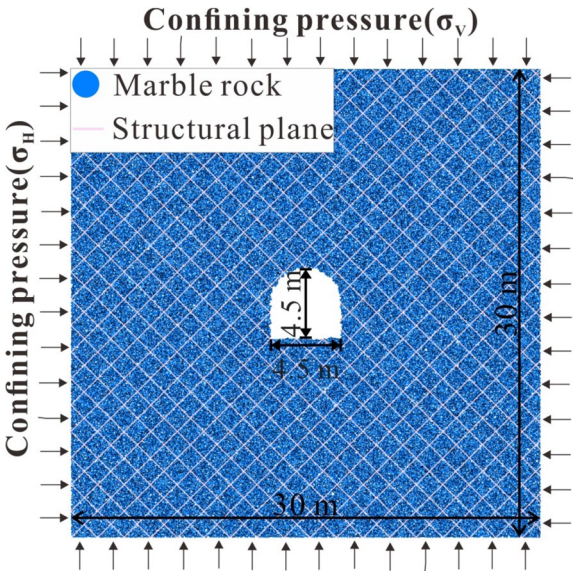

Fig. 13 The numerical simulation model

The PFC model does not permit direct adoption of the macroscopic mechanical parameters of the rock mass, so a calibration model for micromechanical parameters was necessary. Rock parameters and structural plane parameters were grouped and calibrated in this study. Therefore, uniaxial compression tests were conducted on intact rock specimens and rock specimens with structural planes in the study area. Through repeated simulation calculations, the microscopic parameters shown in Table 4 were obtained, and the experimental comparison was shown in Fig. 14.

Servo loading was applied around the model, and geostresses of three different depths were adopted in the numerical calculation, as shown in Table 5.

Numerical simulation results analysis

Based on the numerical model construction approach introduced above, three roadway models in fractured rock mass were developed under different in situ stress with results of the numerical simulation shown in Fig. 15. For roadways in fractured rock mass, several groups of intersecting structural planes were developed in the surrounding rock, cutting the rock mass into independent blocks, which had

Table 4 Microscopic parameters in PFC (Li et al. 2021)

Type	Parameter	Magnitude	Parameter	Magnitude
Particles	Density (kg/m^3)	2500	Young's modulus of particle (GPa)	20
	Minimum particle radius (mm)	60	Ratio of normal to shear stiffness	2
	Ratio of maximum to minimum particle radius	1.67	Friction coefficient	0.5
Parallel Bond	Young's modulus of particle (GPa)	20	Cohesion (MPa)	20
	Ratio of normal to shear stiffness	1	Internal friction angle (°)	25
	Tensile strength (MPa)	20	Bond radius multiplier	1.5
Structural Planes	Cohesion (MPa)	0.1	Tensile strength (MPa)	0.1
	Internal friction angle (°)	25	Tensile strength	1

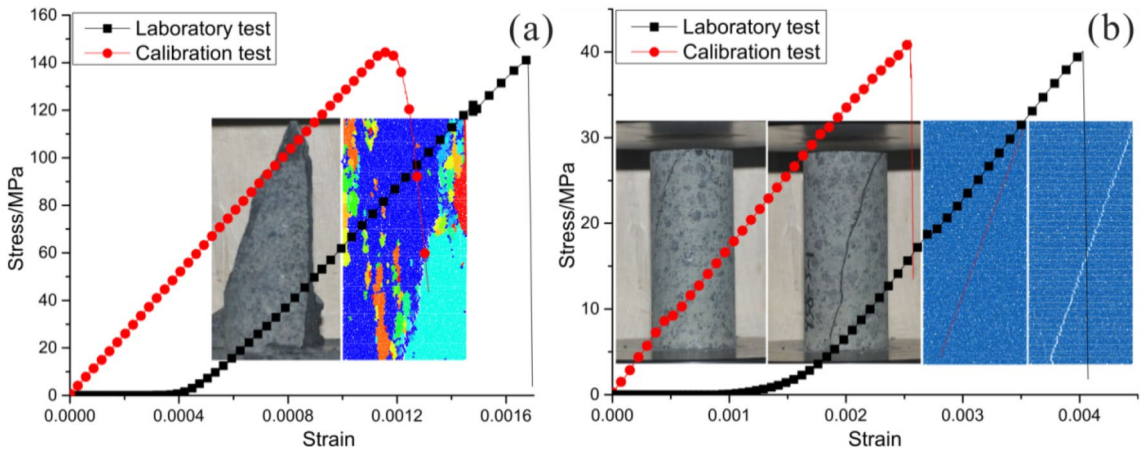

Fig. 14 Calibration results (Li et al. 2021); **a** intact rock and **b** rock with structural plane

Table 5 Geo-stress applied in PFC

Depth (m)	σ_V (MPa)	σ_H (MPa)
550	10	20
750	20	30
1000	30	40

the tendency to slide along the joint planes. Deformation failure modes, mainly including collapse, rock burst, and floor heaving, were similar for roadways of various depths. The wedge blocks located on the right side and roof were extremely unstable, which would break away from the deep surrounding rock as soon as the free surface appeared. If the ground stress was low, the block slid toward the goaf along the structure planes. Instead, the block was thrown to develop a rock burst or collapse. Blocks on the left side were relatively stable, the surrounding rock was squeezed into the goaf with the deformation increasing, forming side cracking and rib spalling. Blocks located on the floor were easily uplifted under the action of in-situ stress, which led to multiple or partial floor heaves. Roadway deformation became more violent and rapid with higher ground stress. Thus, the structure of surrounding rock determined the deformation mode and the geo-stress determined the deformation intensity of roadways.

Displacements on the roof, floor, and two sides of the roadways were recorded, with results shown in Fig. 16.

Total amount and speed of deformation was higher when there was higher ground stress, shown in Fig. 16. Deformations on the left side and floor of the roadway with a buried depth of 550 m were greater, exceeding 20 cm, while the deformations on the right side and roof were lesser, at about 10 cm. Deformation growth rate of each position gradually slowed down and the roadway was stable at the end of the simulation. In the roadway with a depth of 750 m, the deformation on the left side exceeded 75 cm, the right side and floor exceeded 30 cm, and the roof exceeded 15 cm, which increased with varying degrees. Because of the more unstable block combination, the left side had the fastest growth,

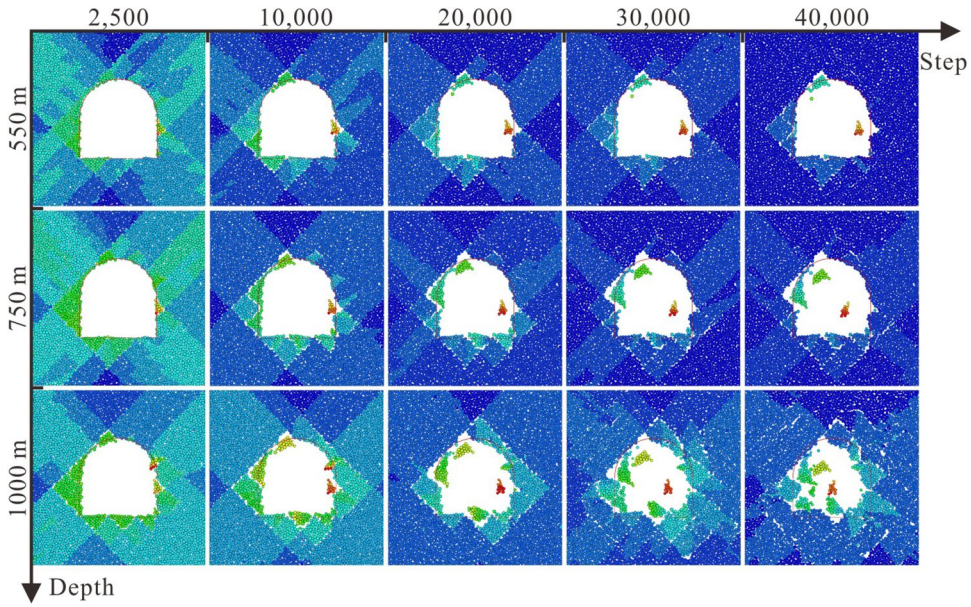

Fig. 15 Results of the numerical simulation

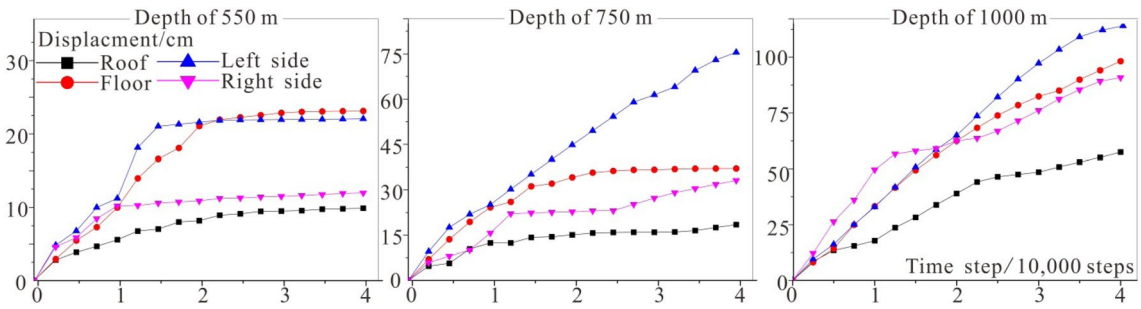

Fig. 16 Displacement–time step curves on important positions of the roadway

while the other parts were all individual block movement. Under the buried depth of 1000 m, the deformation law of each position only slightly changed. The deformation on the left side exceeded 100 cm, and the floor and right side were close to 100 cm. Each position rapidly deformed when the simulated depths were 750 m and 1000 m, especially when the buried depth was 1000 m, because most of the roadway section was occupied by surrounding rocks.

Conclusion

The following conclusions are drawn from a comprehensive comparative analysis of the physical model tests and numerical simulations:

1. A mixed pouring–bricking method most accurately represents the fractured rock failure mechanisms. Pouring was adopted in the inner ring of the model, and bricking was used in the outer ring, which can not only reflect the structural characteristics of jointed surrounding rocks, but also improve the test efficiency. A roadway excavation device (based on an embedded mold) and spiral traction were independently developed to represent the roadway in a model. The physical model based on the roadway in the Jinchuan mining area can truly reproduce the structural characteristics of the prototype and fully replicate the excavation conditions of the roadway, which proves the higher practicability and efficiency of the method. This provides a technical reference for the design and production of similar model experiments.
2. Deformation failure processes of the fractured rock mass roadways with semi-circular arch section were replicated. The deformation initially occurred on the two straight wall feet and the floor. Then, failure appeared at the two sides, blocks fell from the roof, and tensile cracks developed along the roadway trend with continuous increase of the deformation. Additionally, the floor of the roadway cracked and swelled, and the floor gradually heaved, which affected the deeper rock mass. Finally, a peach roof was formed and several considerable scale tensile cracks developed on the two sides, which became the breakthroughs of the surrounding rock converging into the excavated zone.
3. Deformation failure modes of roadways were similar regardless of depths, which mainly included collapse, rock burst, and floor heaving. Roadway deformation became more violent and rapid with the increase of ground stress. The structure of surrounding rock determined the deformation mode and the geo-stress determined the deformation intensity of roadways. Roadway construction in complex geological environments, such as fractured rock masses, requires support technology. A timely first support was needed to prevent initial collapse and rock burst, but a rigid support to ensure the long-term stability of the roadway was also needed.

This study performs experimental research on the deformation failure processes of roadway tunnels in fractured rock masses that are induced by mining excavation. Although several meaningful observations are made, there are still some limitations, as follows. (1) Because the drying time of the physical model test was so long (due to the constraints of the COVID-19 pandemic), the bond strength between blocks was high and resulted in the experiment failing to fully reflect the discontinuity action. (2) The structure plane parameters were not accurately calibrated in the numerical model, so the structural planes were simplified and differed from the actual rock mass structure. In the future, the model can be optimized according to the actual observed joint fracture distribution to truly reflect the deformation failure characteristics of roadway surrounding rock. (3) Both physical and simulation tests were two-dimensional representations of the system, ignoring the influence of one horizontal in-situ stress, and three-dimensional tests should be supplemented in future studies.

Acknowledgements The research received support from the National Natural Science Foundation of China (Grant Nos. 42072305, 41877274, and 41831293). We appreciate the kind support.

Funding All authors agree to submit the paper to this journal. The authors declare that the supporting source had no such involvement.

Declarations

Conflict of interest The authors declare no conflict of interest.

References

An BQ, Tannant DD (2007) Discrete element method contact model for dynamic simulation of inelastic rock impact. Comput Geosci 33(4):513–521. https://doi.org/10.1016/j.cageo.2006.07.006

Bai QS, Tu SH (2020) Numerical observations of the failure of a laminated and jointed roof and the effective of different support schemes: a case study. Environ Earth Sci 79:202. https://doi.org/10.1007/s12665-020-08935-2

Cai M, Kaiser PK, Morioka H, Minami M, Maejima T, Tasaka Y et al (2007) FLAC/PFC coupled numerical simulation of AE in large-scale underground excavations. Int J RockMech Min Sci 44(4):550–564. https://doi.org/10.1016/j.ijrmms.200(6)09.013

Fakhimi A, Carvalho F, Ishida T, Labuz JF (2002) Simulation of failure around a circular opening in rock. Int J Rock MechMin Sci 39(4):507–515. https://doi.org/10.1016/S1365-1609(02)00041-2

He MC, Gong WL, Li DJ et al (2009) Physical modeling of failure process of the excavation in horizontal strata based on IR thermography. Min Sci Technol 19(06):689–698. https://doi.org/10.1016/S1674-5264(09)60128-9

Hendron AJ, Paul Engeling, Aiyer AK et al (1972) Geomechanical model study of the behavior of underground openings in rock

subjected to static loads(report 3)-tests on lined openings in jointed and intact rock. Illinois Univat Urbana Dept of Civil Engineering

Huang F, Zhu HH, Xu QW et al (2013) The effect of weak interlayer on the failure pattern of rock mass around tunnel-Scaled model tests and numerical analysis. Tunn Undergr Space Technol 35:207–218. https://doi.org/10.1016/j.tust.2012.06.014

Hui X, Ma FS, Zhao HJ, Xu JM (2019) Monitoring and statistical analysis of mine subsidence at three metal mines in China. Bull Eng Geol Environ 78:3983–4001. https://doi.org/10.1007/s10064-018-1367-6

Itasca Consulting Group (2008) PFC2D (Particle Flow Code in 2dimensions) users guide. Itasca, Minneapolis

Lee YZ, Schubert W (2008) Determination of the length for tunnel excavation in weak rock. Tunnel Underground Space Technol 23:221–231. https://doi.org/10.1016/j.tust.2007.04.001

Li SC, Wang Q, Wang HT et al (2015) Model test study on surrounding rock deformation and failure mechanisms of deep roadways with thick top coal. Tunnell. Underground Space Technol 47:52–60. https://doi.org/10.1016/j.tust.2014.12.013

Li G, Ma FS, Liu G et al (2019) A strain-softening constitutive model of heterogeneous rock mass considering statistical damage and its application in numerical modeling of deep roadways. Sustainability 11:2399. https://doi.org/10.3390/su11082399

Li G, Ma FS, Guo J et al (2020a) Study on deformation failure mechanism and support technology of deep soft rock roadway. Eng Geol 264:105262. https://doi.org/10.1016/j.enggeo.2019.105262

Li G, Ma FS, Guo J et al (2020b) Deformation characteristics and control method of kilometer-depth roadways in a nickel mine: a case study. Appl Sci 10:3937. https://doi.org/10.3390/app10113937

Li G, Ma FS, Guo J et al (2020c) Experimental study on similar materials ratio used in large scale engineering model test. J Northeastern Univ (natural Science) 41(11):1653–1660. https://doi.org/10.12068/j.issn.1005-3026.2020.11.021 (**Chinese**)

Li G, Ma FS, Guo J et al (2021) Case study of roadway deformation failure mechanisms: field investigation and numerical simulation. Energies 14:1032. https://doi.org/10.3390/en14041032

Liu WR, Wang X, Li CM (2019) Numerical study of damage evolution law of coal mineroadway by particle flow code (PFC) model. Geotech Geol Eng 37:2883–2891. https://doi.org/10.1007/s10706-019-00803-6

Liu SQ, Ma FS, Zhao HJ et al (2020) Numerical analysis on the mechanism of hydraulic fracture behaviour in heterogeneous reservoir under the stress perturbation. J Nat Gas Sci Eng 78:103277. https://doi.org/10.1016/j.jngse.2020.103277

Lu R, Fs Ma, Guo J, Zhao HJ (2018) Monitoring and analysis of ground subsidence and backfill stress distribution in Jinchuan Mine, China. Curr Sci 115(10):1970–1977. https://doi.org/10.18520/cs/v115/i10/1970-1977

Lu R, Fs Ma, Guo J et al (2020) Monitoring and analysis of stress and deformation features of boundary part of backfill in metal mine. Sustainability 12:733. https://doi.org/10.3390/su12020733

Norman Brook (1981) Small scale brittle model studies of mine roadway deformation. In: Farmer IW (eds) Developments in geotechnical engineering, vol. 32. Elsevier, pp 184–189. https://doi.org/10.1016/B978-0-444-42086-2.50035-1

Pf G, Zhang ZP, Wei SJ (2009) Physical simulation test of damage character of surrounding rock under different levels of the horizontal stress. J China Coal Soc. https://doi.org/10.13225/j.cnki.jccs.2009.10.011 (**Chinese**)

Ren FQ, Chang Y, He MC (2020) A systematic analysis method for rock failure mechanism under stress unloading conditions: a case of rock burst. Environ Earth Sci 79:370. https://doi.org/10.1007/s12665-020-09111-2

Shreedharan S, Kulatilake PHSW (2016) Discontinuum–equivalent continuum analysis of the stability of tunnels in a deep coal mine using the distinct element method. Rock Mech Rock Eng 49(5):1903–1922. https://doi.org/10.1007/s00603-015-0885-9

Sun XM, Chen F, Mc He et al (2017) Physical modeling of floor heave for the deep-buried roadway excavated in ten degree inclined strata using infrared thermal imaging technology. Tunnel Underground Space Technol 63:228–243. https://doi.org/10.1016/j.tust.2016.12.018

Tu HS, Tu SH, Wang C et al (2018) Mechanical analysis of a vertical-wall, semicircular-arch roadway and a repair technique using double-shell support. Environ Earth Sci 77:509. https://doi.org/10.1007/s12665-018-7680-3

Wang X, Tian L (2018) Mechanical and crack evolution characteristics of coal–rock under different fracture-hole conditions: a numerical study based on particle flow code. Environ Earth Sci 77(8):297. https://doi.org/10.1007/s12665-018-7486-3

Wang C, Tannant DD, Lilly PA (2003) Numerical analysis of the stability of heavily jointed rock slopes using PFC2D. Int J Rock Mech Min Sci 40(3):415–424. https://doi.org/10.1016/S1365-1609(03)00004-2

Xu YL, Pan KR, Zhang H (2019) Investigation of key techniques on floor roadway support under the impacts of superimposed mining: theoretical analysis and field study. Environ Earth Sci 78:436. https://doi.org/10.1007/s12665-019-8431-9

Zhang MJ, Gao JH, Wei SY et al (2010) Similarity simulation study of failure characteristics of surrounding rocks of tilted strata roadway. Rock Mech Eng 29(1):3259–3326 (**Chinese**)